PNAS
www.pnas.org

Supplementary Information for

Inter-cellular communication induces glycolytic synchronization waves between individually oscillating cells

Martin Mojica-Benavides, David D. van Niekerk, Mite Mijalkov, Jacky L. Snoep, Bernhard Mehlig, Giovanni Volpe, Mattias Goksör, and Caroline B. Adiels.

Caroline B. Adiels.
E-mail: caroline.adiels@physics.gu.se

This PDF file includes:

Figs. S1 to S10
Legends for Movies S1 to S4

Other supplementary materials for this manuscript include the following:

Movies S1 to S4

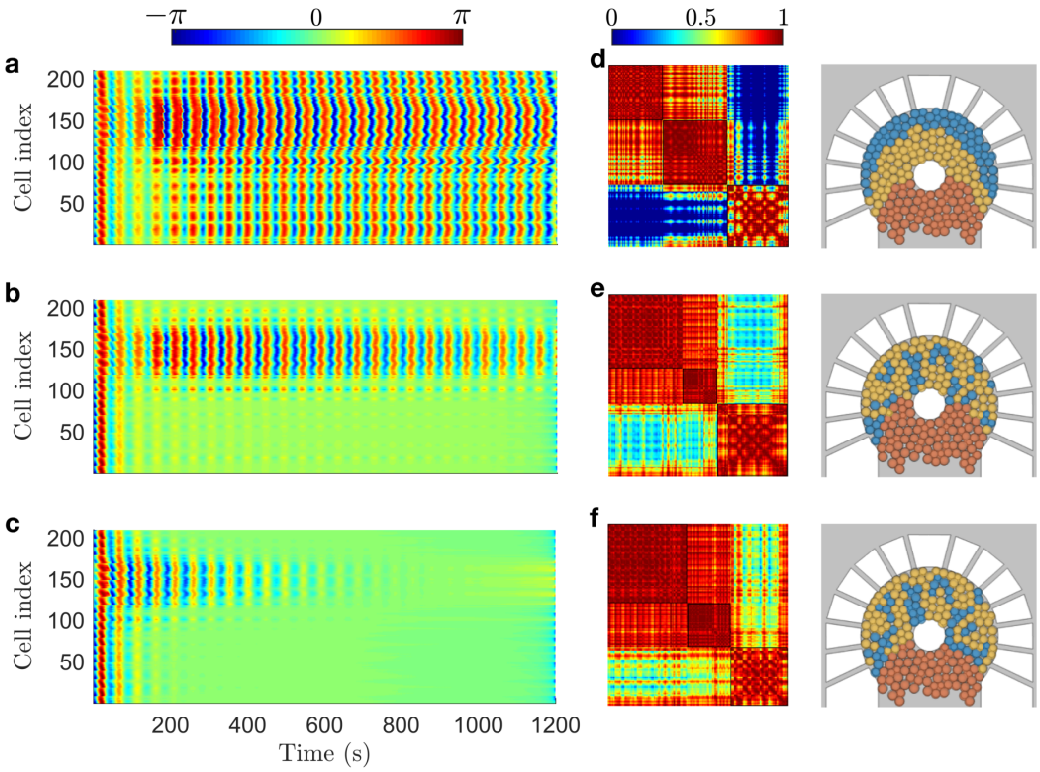

Fig. S1. The kinetic model for single cells predicts the formation of synchronization communities. The 210 simulated cells using the Gustavsson model under the boundary conditions that resembled the experiments, display coupled oscillatory behaviour in the metabolites present through the individual glycolytic pathways. For the CN^- concentrations in the stress solution of (a) 20 mM, (b) 24 mM and (c) 28 mM, NADH instantaneous phases (from -π to π) showed the most distinguishable cases of synchronization distribution across the cell array. (d)- (f) The weighted matrices with Pearson correlation coefficients from 0 to 1 underline the synchronization communities, that emerge shaped by the diffusion gradients from the geometrical conditions. In contrast with the experimental results, a steady state was achieved more homogeneously as cells were exposed to the higher CN^- concentrations, resulting into new non-oscillating communities. Community colors are assigned randomly.

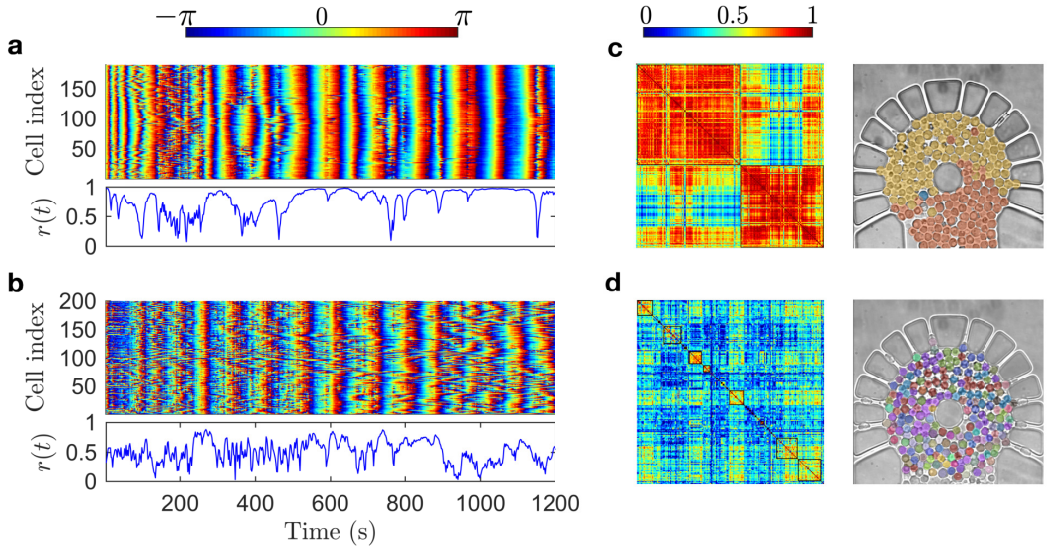

Fig. S2. Synchronization analysis and community structure for the experimental cases of 8 mM and 24 mM of CN^-. (a) For concentrations sufficiently low, glycolytic oscillations are less sustained. Despite the fact that the order parameter r can show higher values, oscillations not necessarily correspond to the glycolytic cycle. (b) Significantly high concentrations of CN^- induce uncorrelated behaviour among the cells as can be noticed from the low values of the order parameter r. (c-d) Present the community structures for these two extreme experimental cases, where the 8 mM case reveal larger communities due to the high presence of secreted ACA. On the other hand in the 24 mM case, a higher amount of ACA is consumed by the binding with CN^- resulting in an undefined community structure. Community colors are assigned randomly.

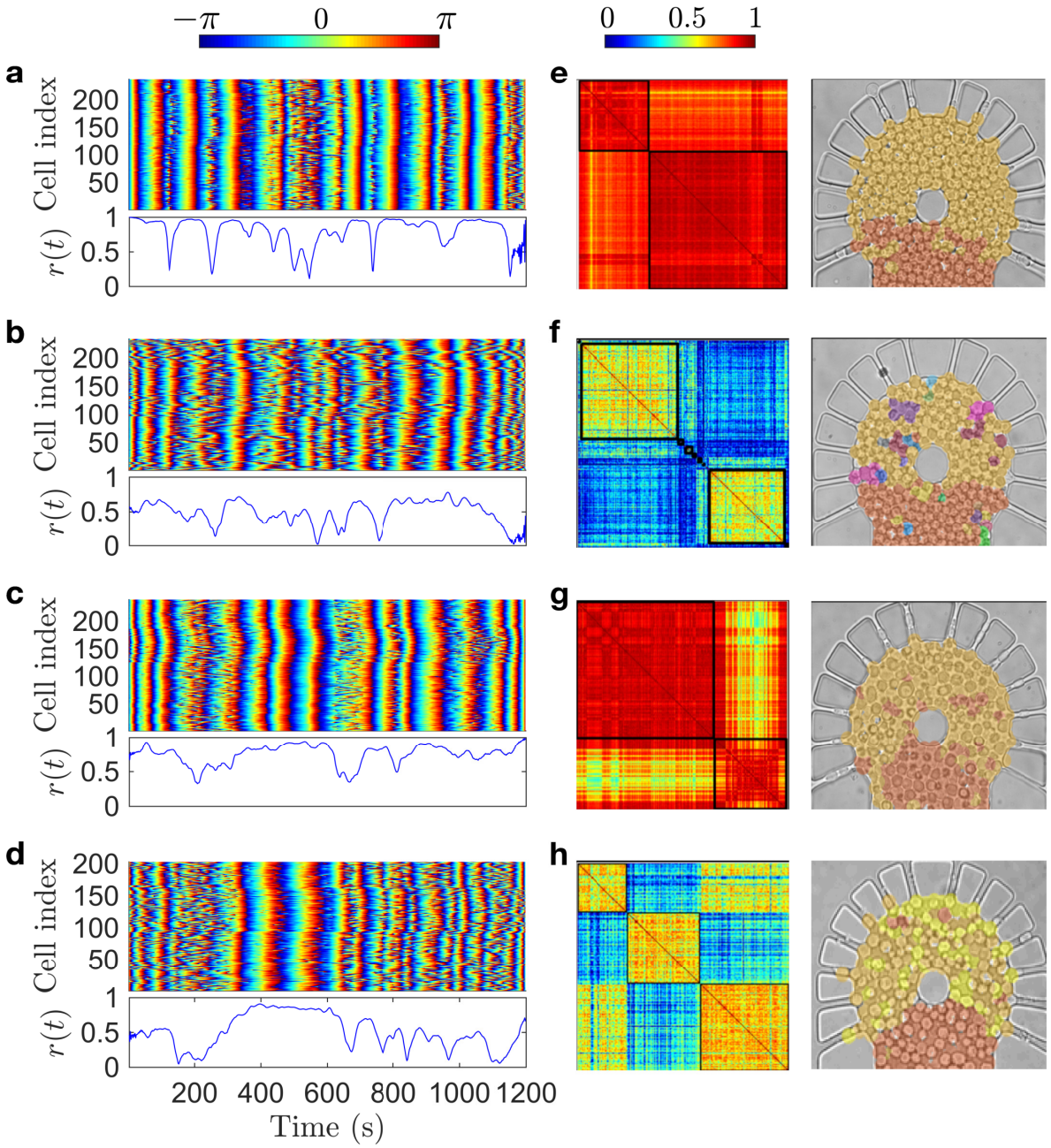

Fig. S3. Community structure repetitions for the 8 mM case.

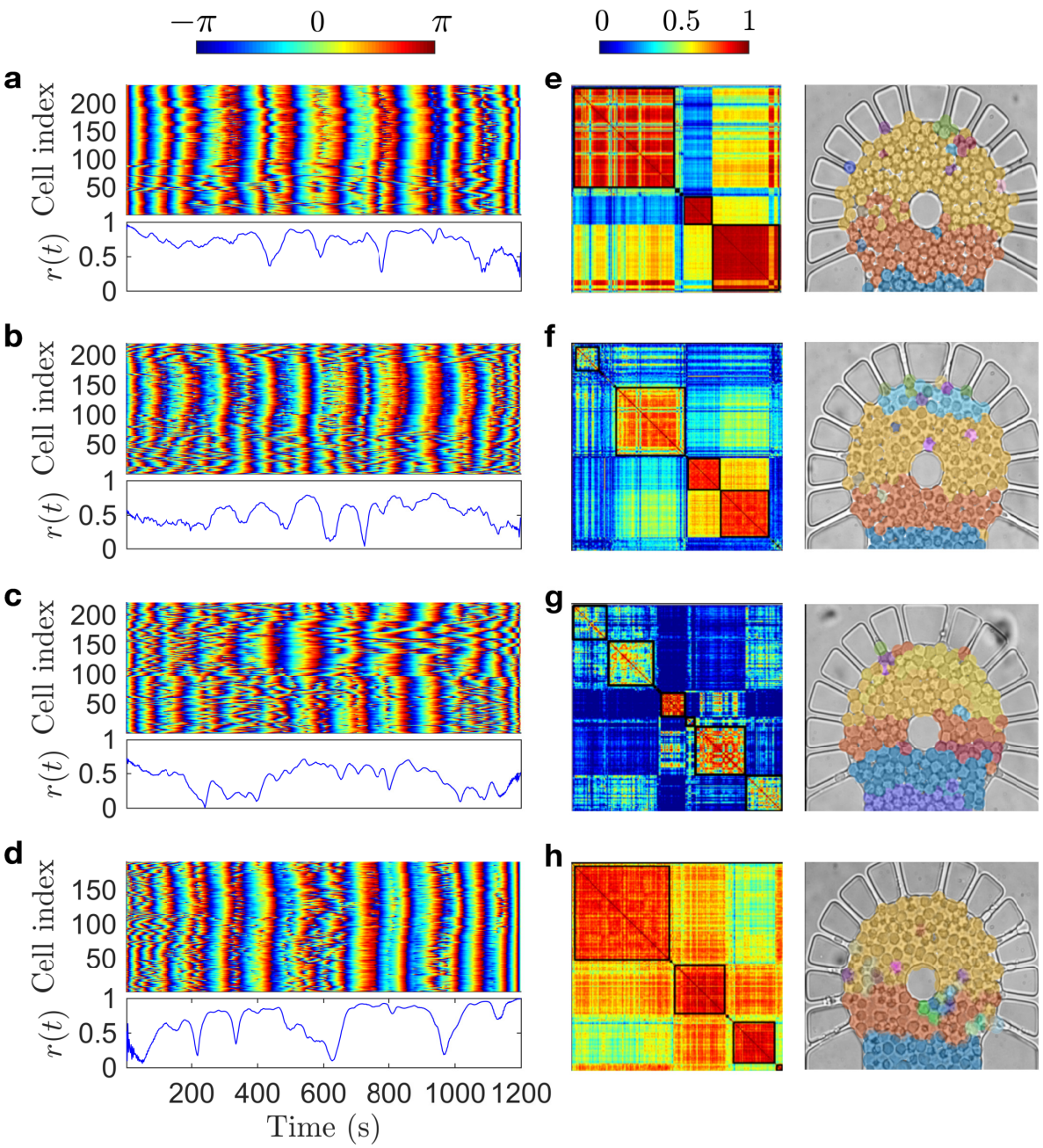

Fig. S4. Community structure repetitions for the 12 mM case.

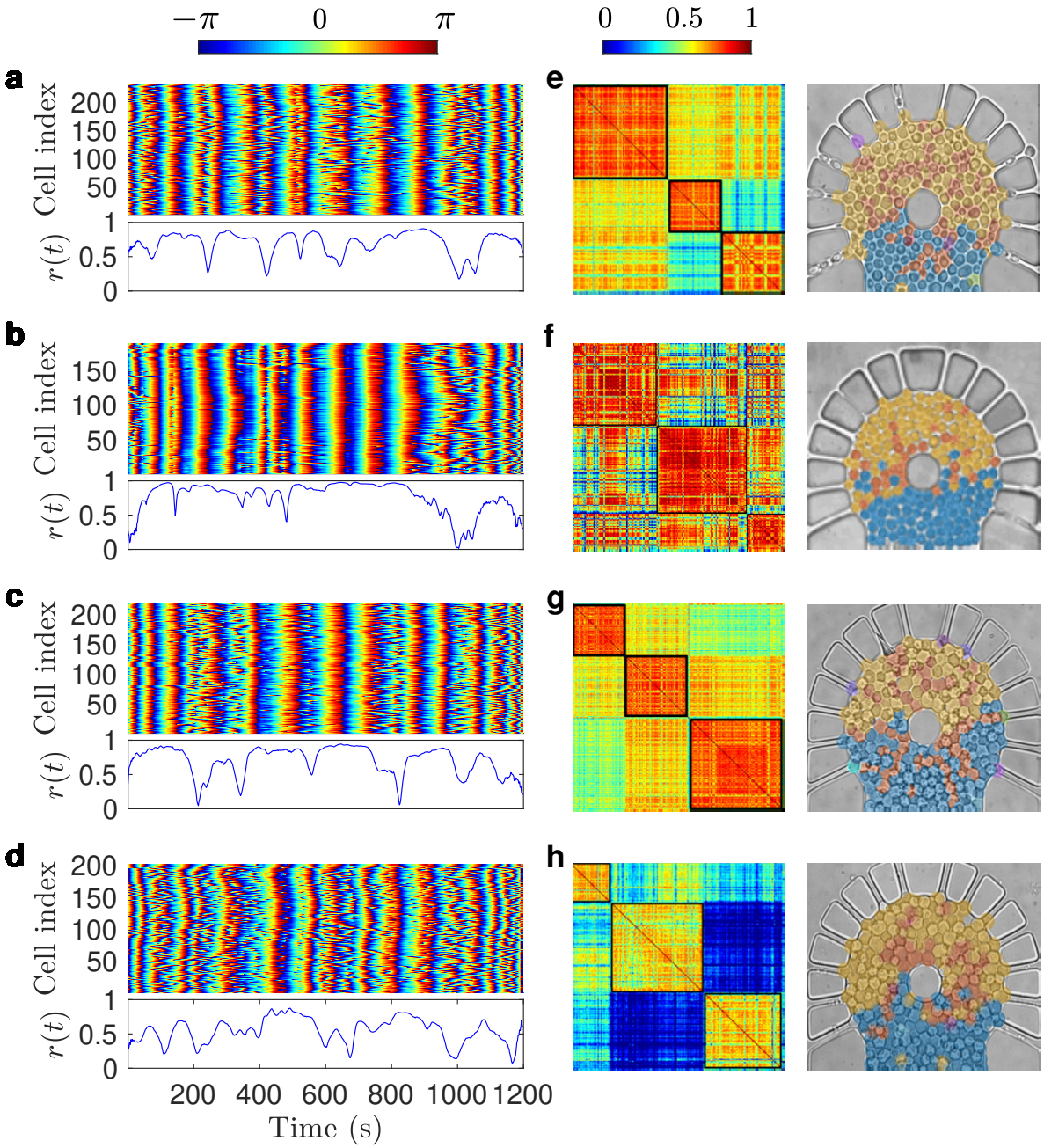

Fig. S5. Repetitions for the 16 mM case.

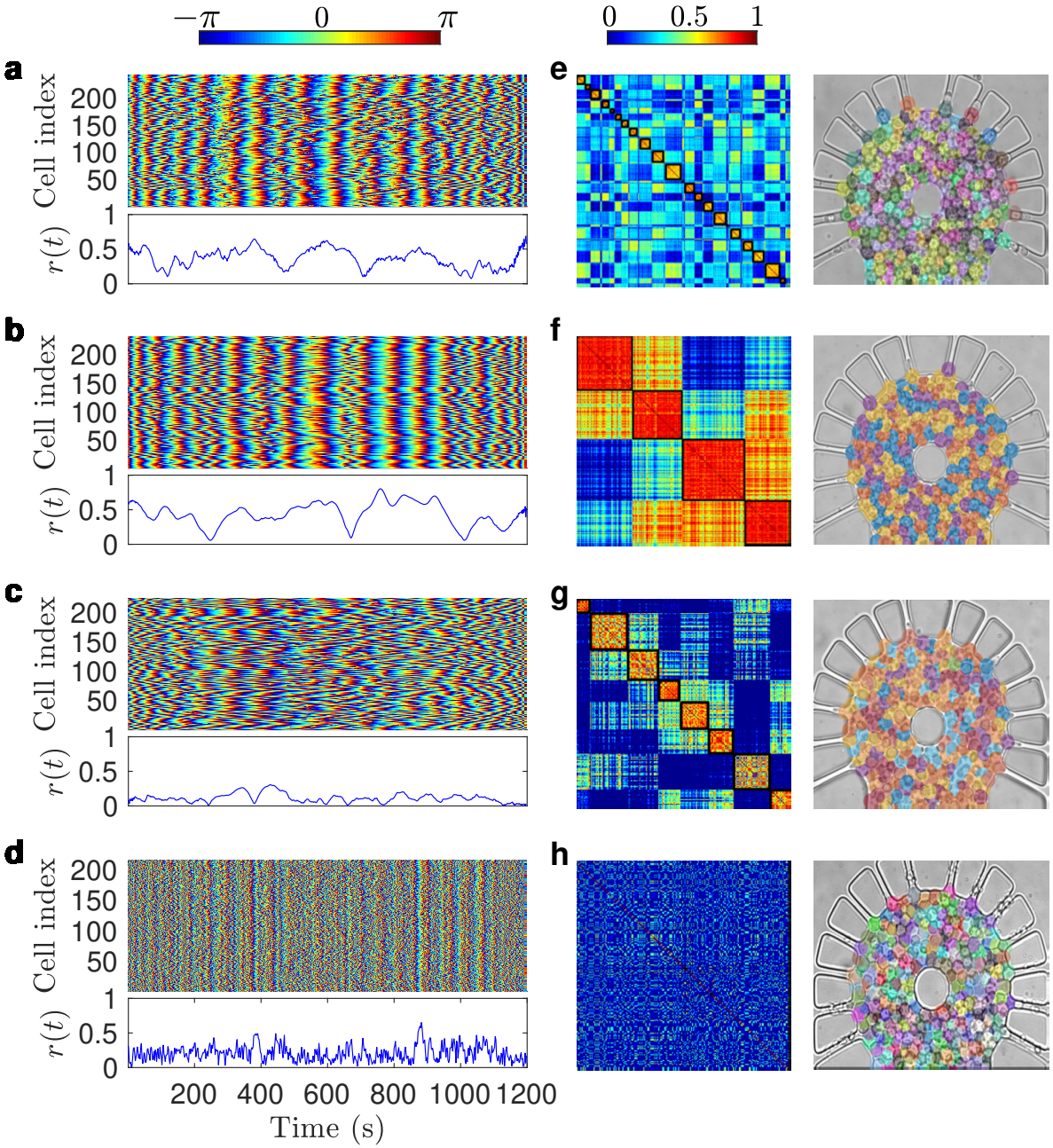

Fig. S6. Community structure epetitions for the 20 mM case.

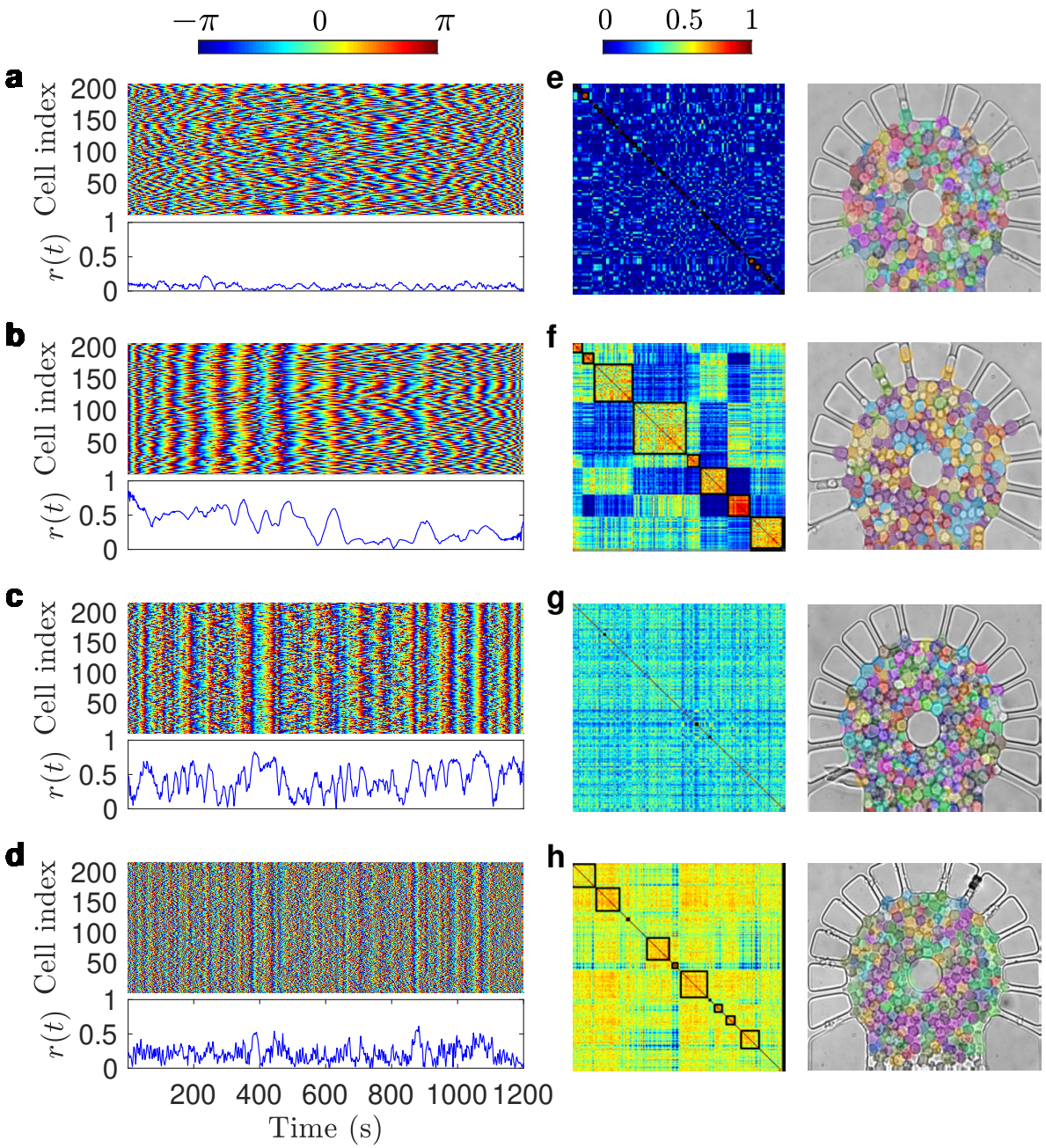

Fig. S7. Community structure repetitions for the 24 mM case.

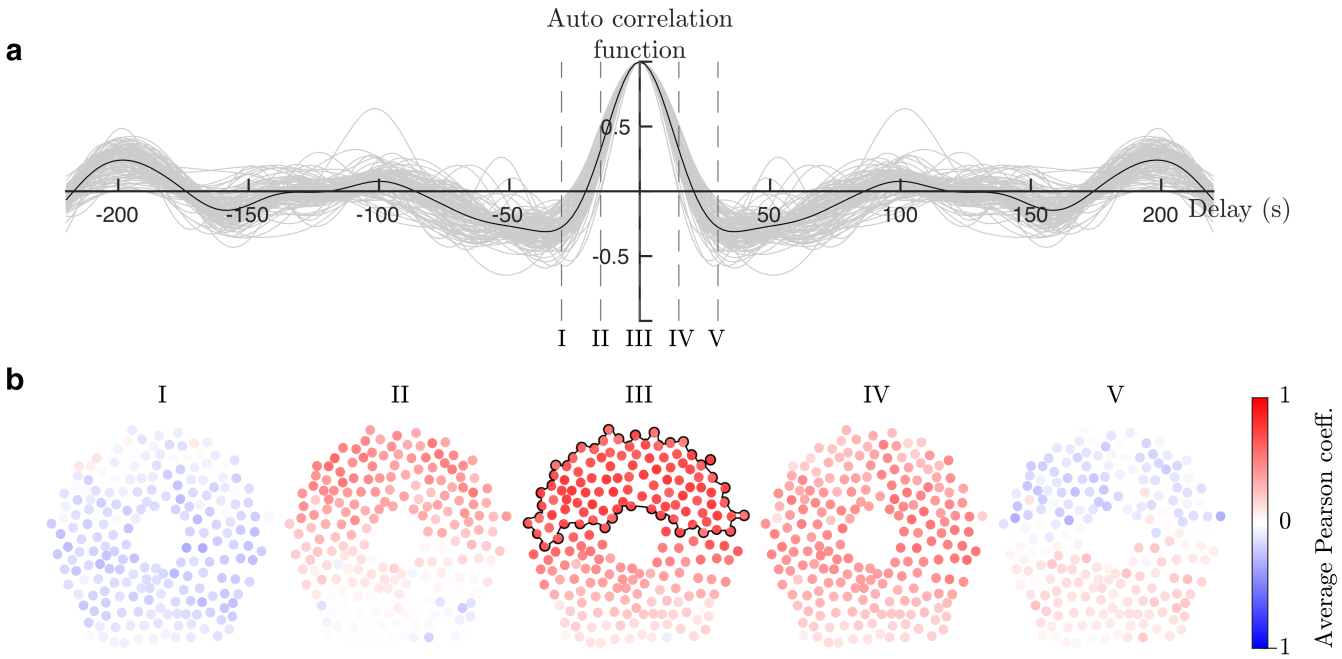

Fig. S8. (a) Auto correlation function and (b) Delayed correlations for the top community in the 12 mM case.

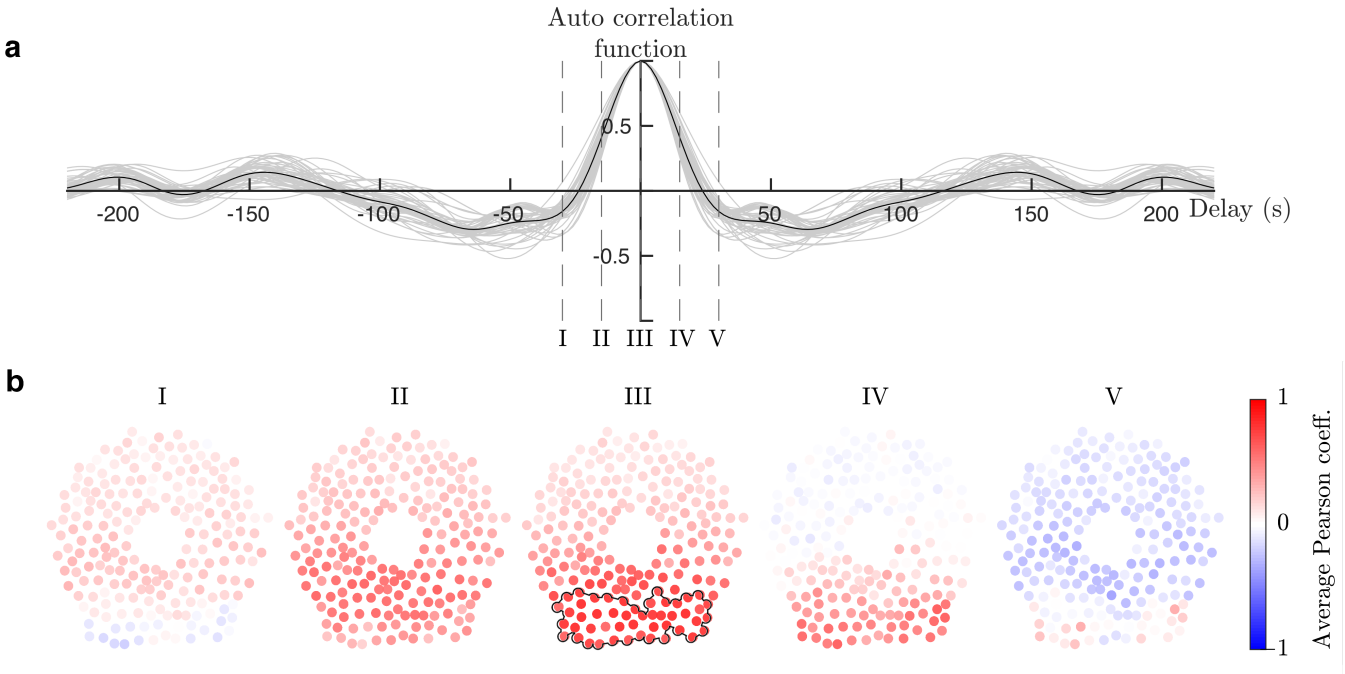

Fig. S9. (a) Auto correlation function and (b) Delayed correlations for the bottom community in the 12 mM case.

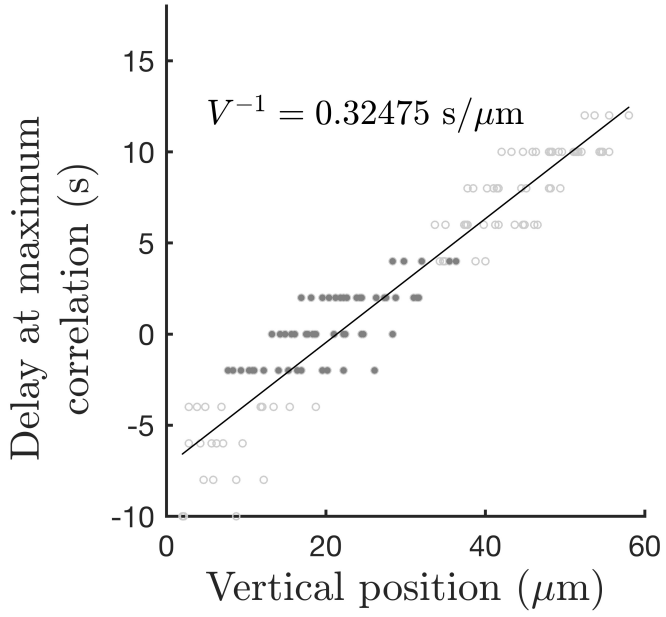

Fig. S10. Simulated wave propagation at 12 mM CN^-. The delay at maximum correlation as a function of vertical position shows a linear relation that confirms a travelling wave. Due to the fact that the simulated waves displayed a more radial-like propagation, only the region of cells covered exclusively by the vertical propagation are used to calculate the regression.

Movie S1. The time-dependent NADH autofluorescence signals show the triggering and posterior synchronization of the glycolytic oscillations with a single-cell resolution. Due to the diffusion-based perfusion of CN^- and GLC synchronization waves spontaneously appear and travel away from the perfusion channels.

Movie S2. The simulated time-dependent ACA and ETOH distributions for external and internal concentrations show distinctive responses depending on the CN^- external concentrations. The coupling resulting from the ACA secretion and exchange, reveal an adaptation to travelling waves that indicate an upper threshold for high CN^-. The ETOH secretions display solely chemical diffusion given that the model does not consider ETOH as a cell-cell coupling agent

Movie S3. The numerical simulations confirm the fast diffusion of external GLC covering the complete monolayer. The homogeneous GLC levels indicate that CN^- diffusion and consumption control the ACA coupling responsible for the traveling waves.

Movie S4. The averaged and normalized delayed correlations between the second community of synchronized cells (marked with black line in Fig. 4) and every cell present in the chamber (red circles) for a cell array exposed to 12 mM CN^-.